Biomolecular sensing using gold nanoparticle–coated ZnO nanotetrapods

Ramakrishna Podila
Department of Physics and Astronomy, Center for Optical Material Science and Engineering Technologies, Clemson University, Clemson, South Carolina 29634

Pengyu Chen
Laboratory of Single-Molecule Biophysics and Polymer Physics, Clemson University, Clemson, South Carolina 29634

Jason Reppert and Apparao M. Rao[a)]
Department of Physics and Astronomy, Center for Optical Material Science and Engineering Technologies, Clemson University, Clemson, South Carolina 29634

Pu Chun Ke[b)]
Department of Physics and Astronomy, Center for Optical Material Science and Engineering Technologies, Clemson University, Clemson, South Carolina 29634; and Laboratory of Single-Molecule Biophysics and Polymer Physics, Clemson University, Clemson, South Carolina 29634

(Received 25 January 2011; accepted 25 April 2011)

Gold nanoparticle–coated ZnO tetrapods have been utilized as a substrate for the detection of fluorescently labeled protein tetramethylrhodamine isothiocyanate bovine serum albumin and phospholipid 1,2-dipalmitoyl-*sn*-glycero-3-phosphoethanolamine-*N*-(Lissamine rhodamine B sulfonyl) down to the concentrations of 15 pM and 79 nM, respectively. Our detection scheme is based on enhanced fluorescence excitation of the biomolecular analytes by the surface plasmon polaritons of gold nanoparticles coated on the ZnO tetrapod whiskers. This enhanced excitation is confirmed using COMSOL Multiphysics, where the optical near field is shown to be dependent on the coating density of the gold nanoparticles and branching of the ZnO nanostructures.

I. INTRODUCTION

Low dimensional metal nanoparticles (NPs) such as Au and Ag exhibit unique optical properties in the visible spectral range because of the excitation of collective electron oscillations known as surface plasmon resonance (SPR). Size, shape, and the arrangement of the metal NPs strongly influence the resonance frequency and, hence, serve as a great tool for tuning optical properties. When metal particles are arranged in a periodic two-dimensional (2D) pattern, incident light induces a coherent interaction between the particles and results in the generation of a plasmon mode with an extremely sharp and strong resonance. Such a resonance may be exploited for long-range communications between metal NPs for biological and chemical sensing. However, fabricating 2D and three-dimensional (3D) geometries of metal NPs generally involves multistep processes and, hence, limits the usage of this extremely sharp coherent SPR. In this article, we describe a straightforward method for preparing AuNP–coated ZnO tetrapods (3D scaffold), which exhibit excellent SPR response to fluorescently labeled protein tetramethylrhodamine isothiocyanate bovine serum albumin (TRITC–BSA) and phospholipid 1,2-dipalmitoyl-*sn*-glycero-3-phosphoethanolamine-*N*-(Lissamine rhodamine B sulfonyl) (Rd–PE), down to the concentrations of 15 pM and 79 nM in aqueous solutions. The use of ZnO nanomaterial was to take advantage of its biocompatibility, rich electrochemistry, high isoelectric point (IEP; ~9.5), and large surface to volume ratio.[1,2] Aside from biological relevance, detection of these two major biomolecular species[3] also helps evaluate the selectivity of the current scheme.

II. EXPERIMENTAL

Figure 1(a) shows a scanning electron microscopy image of ZnO tetrapods prepared by the chemical vapor deposition technique. A ceramic boat containing zinc acetate and zinc metal powders, mixed in a molar ratio of 1:10, was placed in a quartz tube (diameter ~1″; length ~4′) furnace along with Si (100) substrates. The furnace was heated up to 650 °C under the flow of Ar (45 sccm). A gentle flow of O_2 (25 sccm) was introduced 15 min after the temperature was stabilized. The synthesis was carried out for 30 min, and the furnace was cooled down to room temperature under the Ar flow. The as-prepared nanostructures varied in diameter from 50 to 100 nm

Address all correspondence to these authors.
[a)]e-mail: arao@clemson.edu
[b)]e-mail: pcke11@clemson.edu
DOI: 10.1557/jmr.2011.147

 © Materials Research Society 2011

https://doi.org/10.1557/jmr.2011.147 Published online by Cambridge University Press

along the length and were typically 1–3 μm long. Detailed characterizations of the ZnO tetrapods have been provided elsewhere,[4] and no significant impurities were detected in the Energy Dispersive x-ray (EDX) spectra. A Denton vacuum Desk V sputter coater was operated at 45 mA and 50 mTorr for 10 s to coat AuNPs (diameter: 10 nm, from size histogram) onto the tetrapods.

Fluorescently labeled protein TRITC–BSA (molecular weight: 66,860 Da; lyophilized; exitation/emission: 557 nm/576 nm) was purchased from Sigma (Sigma-Aldrich, St. Louis, MO) and diluted in Milli-Q (pH = 6.8; Millipore, Billerica, MA) to a stock concentration of 15 μM. Fluorescently labeled phospholipid Rd–PE (molecular weight: 1249.65 Da; powder; exitation/emission: 571 nm/583 nm) was obtained from Avanti Lipids (Alabaster, AL) and diluted in Milli-Q to a stock concentration of 790 μM. Zeta potential is widely used as a measure of stability of dispersed nanomaterials in suspensions. Thus, we measured the surface charges (zeta potential) of the TRITC–BSA, Rd–PE, ZnO tetrapods, and their mixtures using dynamic light scattering (Nano ZS; Malvern Instruments Inc., Westborough, MA). Specifically, ZnO tetrapods at neutral pH possessed a zeta potential of 15.5 mV, as expected from the high IEP value of ZnO, and it is consistent with that reported for ordered ZnO hierarchical structures.[5] The zeta potentials of the TRITC–BSA and the Rd–PE were −23.6 and −33.8 mV and rose to 0.559 and −23.8 mV when mixed with the ZnO tetrapods. Such reduction in the magnitude of the surface charge (or zeta potential) due to electrostatic interaction between the positively charged ZnO tetrapod whiskers and the negatively charged TRITC–BSA moieties (glutamic acid, aspartic acid) or the Rd–PE lipid head groups suggests good binding between them.

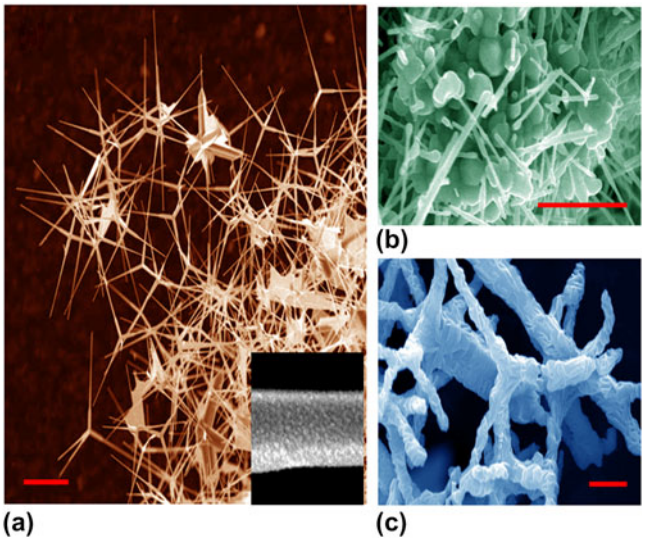


FIG. 1. (a) Scanning electron microscopy (SEM) image of synthesized ZnO tetrapods. Scale bar: 2 μm. Inset: a ZnO whisker coated with AuNPs (shown as granules). (b) SEM image showing globular protein bovine serum albumin (BSA) adsorbed on ZnO tetrapods. Scale bar: 1 μm. (c) SEM image showing ZnO tetrapods fully coated with 1,2-dipalmitoyl-*sn*-glycero-3-phosphoethanolamine-*N*-(Lissamine rhodamine B sulfonyl (Rd–PE) lipids. Scale bar: 1 μm.

TRITC–BSA and Rd–PE solutions, each of 25 μL, were incubated with the AuNP–ZnO tetrapods separately. Figure 1(b) shows prevalent nonspecific binding of the larger globular TRITC–BSA molecules, often encompassing a number of tetrapods and/or tetrapod whiskers. By contrast, Rd–PE molecules were coated mostly on individual ZnO whiskers [Fig. 1(c)]. A Dilor XY triple-monochromator (Horiba-Jobin Yvon, Edison, NJ) was used to excite the fluorescent biomolecules at 514 nm. Figure 2(a) shows the spectra of titrated TRITC–BSA (15 μM–15 pM) mixed with AuNP–ZnO tetrapods in water. In the absence of AuNPs, the fluorescence peak at 575 nm is very weak even for TRITC–BSA of 15 μM in concentration. Interestingly, this fluorescence peak was intensified after AuNP-coated ZnO tetrapods were introduced into the solution and was detectable even at TRITC–BSA of 15 pM in concentration [Fig. 2(c)]. It should be noted that this fluorescence peak (~575 nm) was found to be at least four times weaker for 15 μM of TRITC–BSA when free AuNPs (without ZnO tetrapods) were used [Fig. 2(a)]. In the presence of the AuNPs (distributed on 3D scaffold of ZnO tetrapods) and with an excitation at 514 nm, a new peak appeared at ~530 nm for the biomolecule–ZnO mixture [Figs. 2(a) and 2(b)], corresponding to plasmon polaritons induced on the surfaces of the AuNPs. Such polaritons, arising from 3D architectures of AuNP-coated ZnO tetrapods, could either coherently excite adsorbed fluorescent biomolecules or first be converted to propagating photons by larger AuNP clusters and then excite both adsorbed and nonadsorbed fluorescent biomolecules. A similar trend was observed for the fluorescence peaks at ~580 nm for titrated Rd–PE mixed with AuNP–ZnO tetrapods [Fig. 2(b)], reaching a detection limit of 79 nM for the lipids. It is worth noting that even though the net weight ratios of TRITC–BSA and Rd–PE to ZnO tetrapods were similar, the significantly different sensing molarities partly arose from the different molecular weights of the biomolecules.

III. RESULTS AND DISCUSSION

Figure 2(d) shows fluorescence peak intensities at ~575 nm (~580 nm) as a function of the molarity of TRITC–BSA (Rd–PE). A linear trend was observed above a threshold value of 15 nM (790 nM) in the case of TRITC–BSA (Rd–PE). Below this threshold, the fluorescence rapidly reduced due to the limited availability of biomolecular analytes, which could be excited by the localized and scattered SPR waves. However, even with such limited availability, concentrations as low as 15 pM (79 nM) of TRITC–BSA (Rd–PE) were detectable [Fig. 2(c)]. Such detection limits are significantly lower than those for

https://doi.org/10.1557/jmr.2011.147 Published online by Cambridge University Press

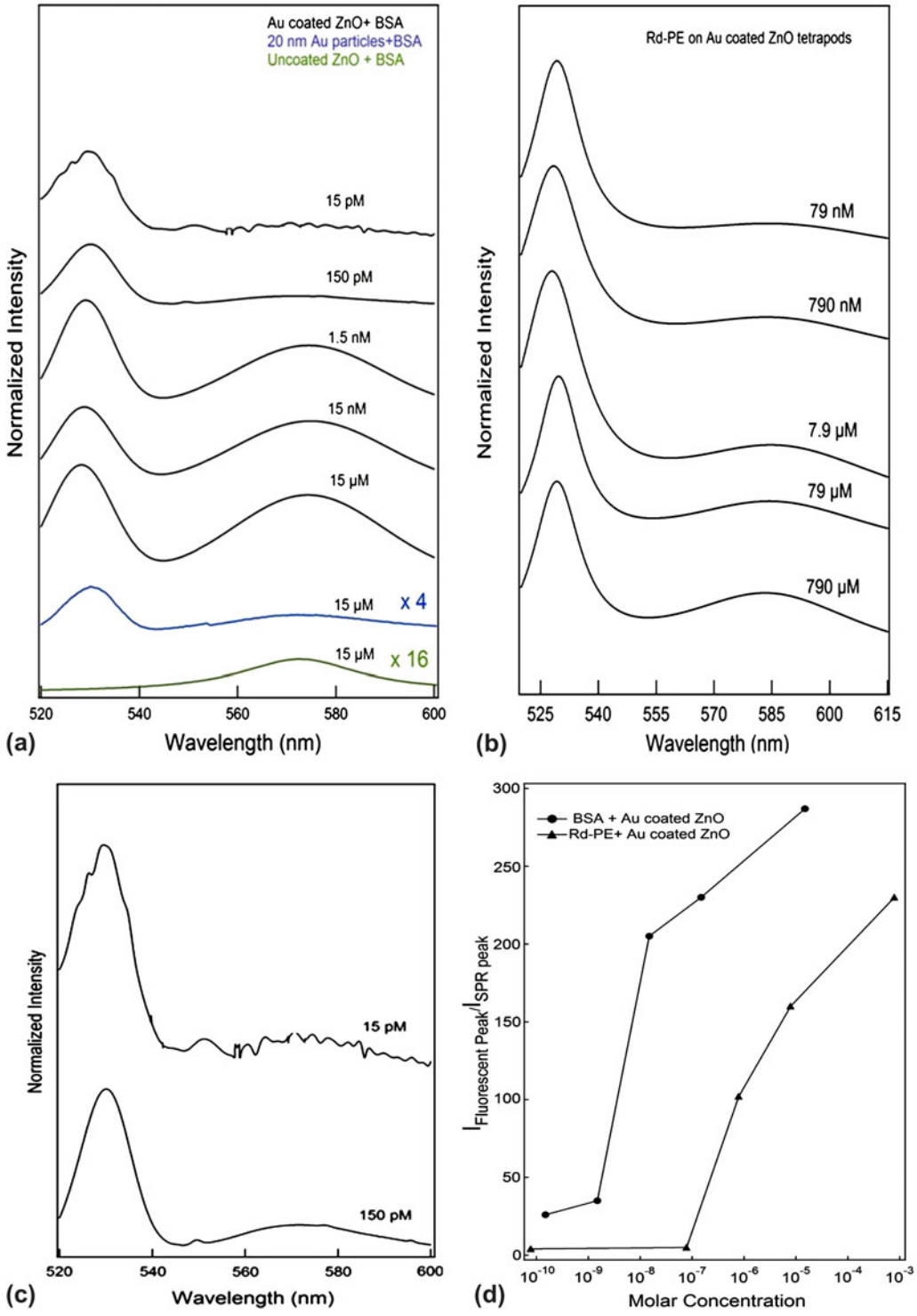


FIG. 2. Surface plasmon resonance (SPR) scattering and fluorescence emission spectra of (a) tetramethylrhodamine isothiocyanate bovine serum albumin (TRITC–BSA) and (b) Rd–PE in aqueous solutions when excited at 514 nm. Fluorescence peaks appear at ~575 nm (~582 nm) for TRITC–BSA (Rd–PE) and the Au plasmon peaks appear at ~530 nm. (c) Magnified spectra of TRITC–BSA of 15 and 150 pM in panel (a). (d) Fluorescence peak intensity versus molar concentration, derived from panels (a) and (b) for TRITC–BSA and Rd–PE.

BSA and ZnO glucose sensors, which had detection limits on the order of micromoles.[2,6]

In addition to charge and molecular weight as discussed above, morphology of the biomolecules could be another key element in determining the binding and, therefore, the detection sensitivity of the current scheme. Although electron microscopy typically depicts dehydrated state, it is still conceivable from Fig. 1(b) that the

https://doi.org/10.1557/jmr.2011.147 Published online by Cambridge University Press

tetrapod junctions and the larger whisker surface areas near the junctions were preferable for the binding of the globular protein BSA ($4 \times 4 \times 14$ nm^3 in dimension). For PE molecules (headgroup width: ~0.6 nm; tail length: ~1 nm), their binding with the tetrapods [Fig. 1(c)] could assume either the random adsorption or the cylindrical micelle model.[7,8] Hemimicellar binding[9] is deemed unfeasible for the organization of PE on ZnO tetrapods, partly because the PE molecules applied in this study were well below their critical micelle concentration (in millimolar range), partly because of the cylindrical steric structure of the PE,[10,11] and partly because of the tapered geometry of the ZnO whiskers, irregular coating of the AuNPs, and the Coulombic attraction between the lipids and the tetrapods, which would disrupt periodic lipid assembly.

To provide a theoretical insight into our experimental scheme, we first calculated the SPR waves on AuNPs. According to Mie theory, for metal particles much smaller than the illumination wave length, the extinction coefficients κ for N number of particles in a volume of V can be expressed as Eq. (1)[12]:

$$\kappa = \frac{18\pi N V \varepsilon_m^{\frac{3}{2}}}{\lambda} \frac{\varepsilon_2}{(\varepsilon_1 + 2\varepsilon_m)^2 + \varepsilon_2^2} \quad , \qquad (1)$$

where λ is the wave length of the illumination light, ε_1 and ε_2 are real and imaginary part of the permittivity of the metal, and ε_m is the dielectric constant of the medium surrounding the particles. From this equation, the resonance condition occurred when $\varepsilon_1 = -2\varepsilon_m$. The effective dielectric constant ε_{eff} for the surrounding aqueous medium of the AuNPs can be derived as[13]:

$$\varepsilon_{eff} = \varepsilon_b \left(\frac{1 + \sigma T/(1+\gamma)}{1 + \sigma T/(1-\gamma)} \right) \quad . \qquad (2)$$

Here ε_b is the dielectric constant of the aqueous solution (1.33 for water), σ (−0.246) is a modified resonance amplifier, and T (−0.25 for spheres) and γ (3 for spheres) are the factors depending on the geometry of the AuNPs. By substituting all the parameters into Eqs. (2), ε_{eff} was calculated to be 1.394. Based on Eqs (1) and (2), the resonance wave length was derived to be 515 nm, shorter than the SPR wave length of 530 nm as observed in the experiment (Fig. 2). This discrepancy can be attributed to the shape anisotropy and nonuniform coating of the AuNPs on the ZnO tetrapods and the large AuNP clusters which induced red-shifts of the SPR peaks.[14]

In consideration of computational cost, we performed simulations on the *2D projections* of ZnO tetrapods (referred as *tripods*) with a refractive index of 2.2. Although such simplifications may not provide an accurate quantification of AuNP-induced field enhancement, they can be used to qualitatively explain our experimental observations. To verify AuNP-induced field enhancement, we used COMSOL Multiphysics (COMSOL INC., Los Angeles, CA) to simulate the optical responses for the following three cases in water: (i) bare ZnO tripod, (ii) ZnO tripod with periodic coating of AuNPs, (iii) a ZnO tripod randomly coated with AuNPs, and (iv) ZnO tripod versus a ZnO nanowire, both coated with similar AuNP coverages. The simulation system with randomly coated AuNPs is illustrated in Fig. 3(a). Specifically, a TM-polarized plane wave of 514 nm was incident from the left side of the nanostructure, and the ZnO tripod was set to be 30 nm in size at the junction and tapered to zero at the tip. The width of the ZnO nanowire was set to be 30 nm uniformly along the length of the nanowire with no tapering. The length of each ZnO tripod whisker or the entire ZnO nanowire was 1 μm. The AuNPs were considered hemispheres of 10 nm in diameter following the observation by Li et al.[15] The permittivity of the AuNPs was chosen to be $-3.8 + 2.6i$,[16] and the number of the AuNPs bound on each ZnO tripod whisker was fixed to be 32. A perfectly matched layer boundary condition[17] was adopted to eliminate unnecessary reflections by the simulation box.

Figure 3(b) illustrates intense SPR fields near the sharp tips and junctions of the ZnO tripod shown in Fig. 3(a). These fields were enhanced through the coupling or constructive interference of the SPR waves of adjacent AuNPs coated on the same or neighboring ZnO tripod whiskers [white arrows in Fig. 3(b)]. To quantify our simulation results, a baseline was set 10 nm away from the apices of the AuNPs and the intensities along this line were plotted as a function of distance from the junction of the ZnO tripod (junction being the origin) or the right end of the ZnO nanowire. We further derived average near-field peak intensity $\bar{I} = \frac{\sum (E^2)_{peak}}{N}$, where E denotes the maximum field amplitude at the chosen baseline, and N the number of peaks along the entire length of the ZnO tripod/nanowire.

As expected, we do not observe any plasmonic coupling for a bare ZnO tripod as the AuNPs are absent. Importantly, we observe that the constructive coupling of plasmon waves (or the local enhancement of the electric field) occurs for both periodic *as well as randomly distributed* AuNPs on ZnO tripods. Further, our simulations indicate that constructive coupling is relatively enhanced by 72% in (branched) ZnO tripods compared with that in (unbranched) ZnO nanowires.

Figure 3(c) compares the near-field intensities for a ZnO tripod (red line) and an unbranched ZnO nanowire (dashed green line), both coated with AuNPs (spaced 50 nm apart) of the same coverage density. Especially near the junction (the left two peaks of the red line) and the sharp tip (the right two peaks of the red line) of the tripod, the near-field intensities were much more pronounced than those for the nanowire, increased by 72.8% in terms of the average near-field peak intensity $\bar{I}$. This result indicates that near

https://doi.org/10.1557/jmr.2011.147 Published online by Cambridge University Press

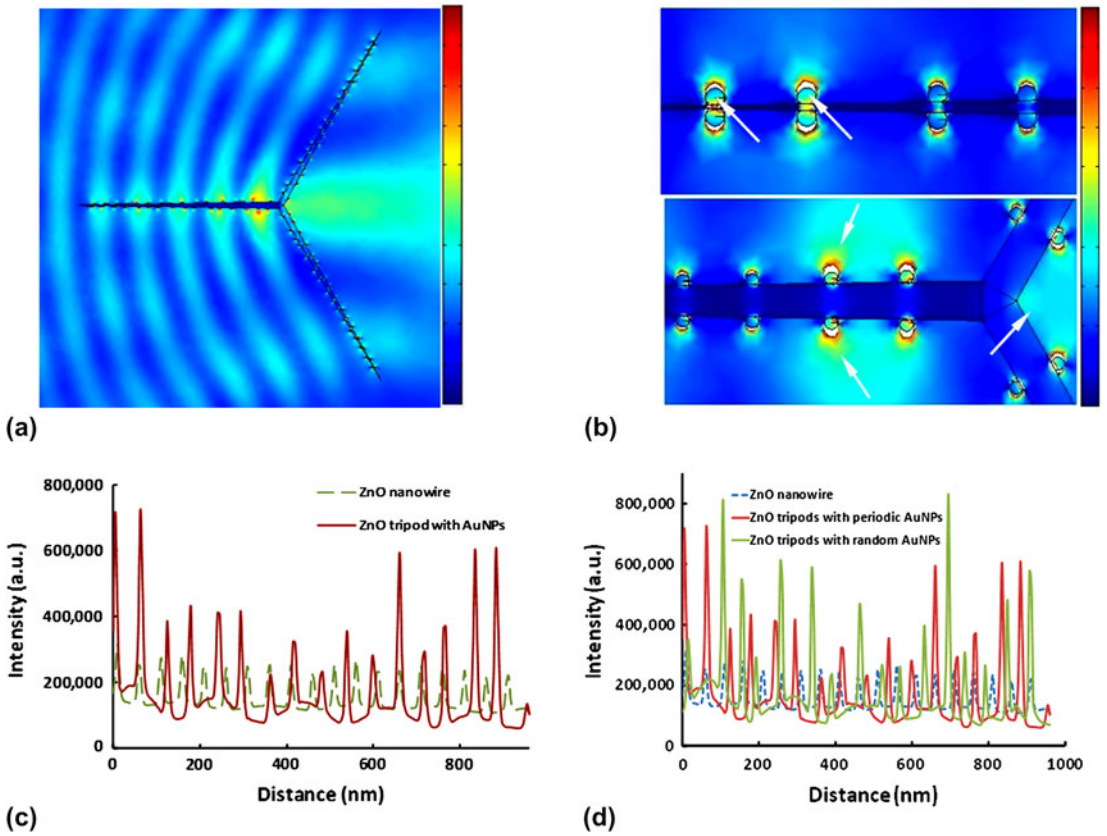


FIG. 3. (a) Simulation of electric field propagating from left to right near a random AuNP distribution on ZnO tripod in aqueous solution. (b) Zoomed-in views of the coupling-enhanced electric fields near the sharp tip (white arrows) and junction of the ZnO tripod (white arrows point to higher intensity regions) in (a). (c) Comparison of the SPR fields for a ZnO nanowire versus a ZnO tripod, both coated with AuNPs of 50 nm in gap size. Distance zero corresponds to the junction of the ZnO tripod or the right end of the ZnO nanowire. (d) Comparison of the SPR fields for a ZnO tripod randomly coated with AuNPs (red). The optical near field for a ZnO nanowire and tripod coated with AuNPs of 50-nm periodicity (blue and green).

field can be strengthened by increasing the branching of ZnO nanostructures.

Since SPR is a physical phenomenon associated with metallic NPs or thin films, we compared the optical near fields for the randomly and periodically (with a periodicity of 25 and 50 nm) distributed AuNPs on ZnO tripods. We observed that AuNPs show overall enhanced fields irrespective of their distribution or periodicity on the tripods [sharp peaks in Fig. 3(d)]. No such peaks were observed for the tripod in the absence of AuNPs (data not shown). We also investigated the effect of AuNP coating density on the SPR enhancement. It is interesting to note that a greater near field (by 31% in terms of the average near-field peak intensity) was induced by AuNPs that were spaced 25 nm apart (green) compared with the ones placed 50 nm apart (red). Such enhancement may be due to the more effective SPR wave coupling between closely spaced neighboring AuNPs.

IV. CONCLUSIONS

In short, both our experimental and simulation results indicate that SPR waves can be enhanced and optimized by increasing branching of the ZnO nanostructures and coating density of randomly distributed AuNPs. Although not examined in this paper, other aspects such as the size of the AuNPs and spatial organization of the ZnO tetrapods could also play important roles in providing more efficient and localized excitation for fluorescent biomolecules, further improving fluorescence emission and sensing by the current experimental scheme.

ACKNOWLEDGMENTS

This research was sponsored by NSF CAREER Award No. CBET-0744040 and U.S. Environmental Protection Agency Grant No. R834092 to P.C. Ke. The authors thank Dr. Thompson Mefford and Dr. Terry Tritt for the use of the zeta potential device and the gold sputtering system.

REFERENCES

1. Y. Gu, J. Zhou, W. Mai, Y. Dai, G. Bao, and Z.L. Wang: Measuring the transport property of ZnO tetrapod using in situ nanoprobes. *Chem. Phys. Lett.* **484**, 96 (2010).

https://doi.org/10.1557/jmr.2011.147 Published online by Cambridge University Press

2. S.A. Kumar and S.M. Chen: Nanostructured zinc oxide particles in chemically modified electrodes for biosensor applications. *Anal. Lett.* **41**, 141 (2008).
3. D.C. Carter and J.X. Ho: Structure of serum albumin. *Adv. Protein Chem.* **45**, 153 (1994).
4. R. Podila, W. Queen, A. Nath, A. Fazzio, A. Schonalez, J. He, G. Dalpian, M.J. Skove, S.J. Hwu, and A.M. Rao: Origin of FM in pristine micro- and nanostructured ZnO. *Nano Lett.* **10**, 1380 (2010).
5. J-H. Lee, I.-C. Leu, Y.-W. Chung, and M-H. Hon: Fabrication of ordered ZnO hierarchical structures controlled via surface charge in the electrophoretic deposition process. *Nanotechnology* **17**, 4445 (2006).
6. M-W. Shao, H. Yao, M.-L. Zhang, N.-B. Wong, Y.-Y. Shan, and S-T. Lee: Fabrication and application of long strands of silicon nanowires as sensors for bovine serum albumin detection. *Appl. Phys. Lett.* **87**, 183106 (2005).
7. C. Richard, F. Balavoine, P. Schultz, T.W. Ebbesen, and C. Mioskowski: Supramolecular self-assembly of lipid derivatives on carbon nanotubes. *Science* **300**, 775 (2003).
8. P.C. Ke: Fiddling the string of carbon nanotubes with amphiphiles. *Phys. Chem. Chem. Phys.* **9**, 439 (2007).
9. R. Qiao and P.C. Ke: Lipid-carbon nanotube self-assembly in aqueous solution. *J. Am. Chem. Soc.* **128**, 13656 (2007).
10. Y. Wu, J.S. Hudson, Q. Lu, J.M. Moore, A.S. Mount, A.M. Rao, E. Alexov, and P.C. Ke: Coating single-walled carbon nanotubes with phospholipids. *J. Phys. Chem. B* **110**, 2475 (2006).
11. S. Lin, G. Keskar, Y. Wu, X. Wang, A.S. Mount, S.J. Klaine, J.M. Moore, A.M. Rao, and P.C. Ke: Detection of phospholipid-carbon nanotube translocation using fluorescence energy transfer. *Appl. Phys. Lett.* **89**, 143118 (2006).
12. G.C. Papavassiliou: Optical properties of small inorganic and organic metal particles. *Prog. Solid State Chem.* **12**, 185 (1980).
13. K.C. Vernon, A.M. Funston, C. Novo, D.E. Gómez, P. Mulvaney, and T.J. Davis: Influence of particle−substrate interaction on localized plasmon resonances. *Nano Lett.* **10**, 2080 (2010).
14. S. Link and M.A. El-Sayed: Spectral Properties and Relaxation Dynamics of Surface Plasmon Electronic Oscillations in Gold and Silver Nanodots and Nanorods. *J. Phys. Chem. B* **103**, 8410 (1999).
15. C. Li, L. Li, Z. Du, H. Yu, Y. Xiang, Y. Li, Y. Cai, and T. Wang: Rapid and ultrahigh ethanol sensing based on Au-coated ZnO nanorods. *Nanotechnology* **19**, 035501 (2008).
16. P.B. Johnson and R.W. Christie: Optical constants of the noble metals. *Phys. Rev. B: Condens. Matter* **6**, 4370 (1972).
17. P. Chen, Q. Gan, F. Bartoli, and L. Zhu: Spoof-surface-plasmon assisted light beaming in mid-infrared. *J. Opt. Soc. Am. B: Opt. Phys.* **27**, 685 (2010).

https://doi.org/10.1557/jmr.2011.147 Published online by Cambridge University Press